Four homobinuclear lanthanide complexes with 3-D coordination networks based on 3-methyloxysalicylaldoxime: syntheses, crystal structures, and properties

Tiantian Yao, Suna Wang, Dacheng Li & Jianmin Dou

⊞ View supplementary material ⬚

📅 Accepted author version posted online: 20 Jan 2015.
Published online: 17 Feb 2015.

✎ Submit your article to this journal ⬚

📊 Article views: 68

🔍 View related articles ⬚

CrossMark View Crossmark data ⬚

Taylor & Francis
Taylor & Francis Group

Four homobinuclear lanthanide complexes with 3-D coordination networks based on 3-methyloxysalicylaldoxime: syntheses, crystal structures, and properties

TIANTIAN YAO, SUNA WANG, DACHENG LI* and JIANMIN DOU*

Shandong Provincial Key Laboratory of Chemical Energy Storage and Novel Cell Technology, School of Chemistry and Chemical Engineering, Liaocheng University, Liaocheng, PR China
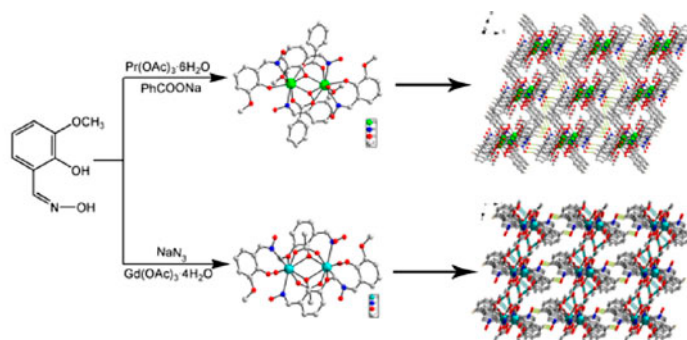
Four new homobinuclear lanthanide(III) complexes of multidentate 3-methyloxysalicylaldoxime (MeOsaloxH$_2$), [Ln$_2$(MeOsaloxH)$_4$(PhCOO)$_2$(CH$_3$OH)$_2$] (Ln = Pr, **1**; Nd, **2**; Sm, **3**) and [Gd$_2$(MeOsaloxH)$_4$(CH$_3$COO)$_2$(H$_2$O)$_2$]·2H$_2$O (**4**), have been synthesized and characterized by elemental analyses, IR spectroscopy, and single-crystal X-ray diffraction. In these complexes, the two Ln^{III} ions are bridged by two phenolate oxygens from two $\eta^1:\eta^2:\eta^1:\mu_2$-[MeOsaloxH]$^-$ ligands and two carboxylate groups to form a [Ln$_2$O$_2$(RCOO)$_2$] binuclear structure (R = Ph, **1–3**; CH$_3$, **4**). The noncovalent interactions (hydrogen bonds and weak C–H···O interactions) led to two types of 3-D supramolecular architectures. Magnetic and luminescence properties of these complexes have also been studied.

Keywords: Lanthanide complexes; 3-Methyloxysalicylaldoxime; Crystal structure; Supramolecular architecture

1. Introduction

Self-assembly of coordination polymers and metallo-supramolecular architectures through crystal engineering has attracted attention for structural versatility, special properties, and applications in different areas, such as nanotechnology and materials [1–6]. Noncovalent

---

*Corresponding authors. Email: lidacheng@lcu.edu.cn (D. Li); dougroup@163.com (J. Dou)

interactions, such as hydrogen bonds, weak C–H···X (X = O, N, F, Cl, π) interactions [7, 8], and π–π stacking interactions [9, 10], play important roles in self-assembly of the network structure. Therefore, self-assembly of coordination polymers and inorganic architectures with the function of the noncovalent interactions is an active theme [11–14].

Incorporation of trivalent lanthanide ions into the molecular architecture has received interest due to their interesting magnetism [15–19], luminescent properties [20, 21], and potential applications [22, 23], such as adsorption, separation, catalysis, sensor, and molecular recognition. With larger size, more flexible coordination geometry, and higher coordination numbers [24], trivalent lanthanide ions are good choices for building multi-dimensional coordination polymers and metallo-supramolecular architectures compared to transition metals. Selection of the multidentate organic ligand is a key point to design and assemble expected polymers. A simple and suitable multidentate ligand 3-methyloxysalicylaldoxime (MeOsaloxH$_2$) has been employed, which may be favorable for the formation of lanthanide complexes through both potential single-atom (O$_{phenolate}$) and two-atom (N–O$_{oxime}$) bridges. For example, a unique Dy$_7$ cluster [25] and a family of linear Dy$_3$ clusters [26] based on MeOsaloxH$_2$ have been reported, and Dy$_3$ species behave as single-molecule magnets. Moreover, the versatile coordination binding modes of the oxime group along with hydrogen bond donor and acceptor properties are helpful for assembling supramolecular architectures [27, 28].

Here, we report four new homobinuclear lanthanide(III) complexes, [Ln$_2$(MeO-saloxH)$_4$(PhCOO)$_2$(CH$_3$OH)$_2$] where Ln = Pr (**1**), Nd (**2**), Sm (**3**), and [Gd$_2$(MeO-saloxH)$_4$(CH$_3$COO)$_2$(H$_2$O)$_2$]·2H$_2$O (**4**), which have been synthesized from reactions of Ln(OAc)$_3$·nH$_2$O (*n* = 6, **1–3**; 4, **4**) with the polydentate MeOsaloxH$_2$ ligand in methanol solution. Magnetic and luminescence properties of these complexes have also been studied.

2. Experimental

2.1. *Materials and physical measurements*

All reactions were performed under aerobic conditions. Reagents and solvents were commercially available and used as received. MeOsaloxH$_2$ was synthesized as described [29]. *Caution!* Care should be taken when using the potentially explosive azide compounds.

C, H, and N microanalyses were carried out with an Elementar Vario-EL CHNS elemental analyzer. IR spectra were recorded as KBr from 4000 to 400 cm^{-1} on a Nicolet-5700 FT-IR spectrometer. Magnetic measurements were carried out with the use of a Quantum Design MPMS SQUID-VSM magnetometer. Measurements were performed on microcrystalline samples. The susceptibility measurement was performed from 300 to 1.8 K with an applied field of 1000 Oe. Diamagnetic corrections were estimated from Pascal's constants [30]. Fluorescence spectra were measured at room temperature with the steady state and time-resolved fluorescence spectrometer.

2.2. *Preparation*

2.2.1. Synthesis of [Ln$_2$(MeOsaloxH)$_4$(PhCOO)$_2$(CH$_3$OH)$_2$] (Ln = Pr (1), Nd (2) and Sm (3)). MeOsaloxH$_2$ (0.067 g, 0.4 mM) and sodium benzoate (0.058 g, 0.4 mM) were dissolved in methanol (30 mL). The solution was then stirred for 1 h and Ln(OAc)$_3$·6H$_2$O (0.4 mM) and triethylamine (0.04 g, 0.8 mM) were added. After stirring for 4 h, the

solution was filtered and the filtrate was left undisturbed to give green crystals (yield: 0.059 g, 47%, based on MeOsaloxH$_2$) of **1**, lilac crystals (yield: 0.038 g, 30%, based on MeOsaloxH$_2$) of **2** and buff crystals (yield: 0.051 g, 40%, based on MeOsaloxH$_2$) of **3** [scheme 1(a)].

For **1**, Anal. Calcd for C$_{48}$H$_{50}$N$_4$O$_{18}$Pr$_2$ (%): C, 46.02; H, 4.02; N, 4.47. Found: C, 45.89; H, 3.93; N, 4.56. IR (KBr, cm^{-1}): 3418(s), 1634(m), 1456(m), 1386(m), 1337(w), 1292(m), 1244(m), 1217(m), 1080(m), 960(m), 855(w), 725(m).

For **2**, Anal. Calcd for C$_{48}$H$_{50}$N$_4$Nd$_2$O$_{18}$ (%): C, 45.78; H, 4.00; N, 4.45. Found: C, 45.83; H, 3.92; N, 4.53. IR (KBr, cm^{-1}): 3455(s), 1634(m), 1463(m), 1385(m), 1337(w), 1292(w), 1243(w), 1219(w), 1080(w), 962(w), 855(w), 724(m).

For **3**, Anal. Calcd for C$_{48}$H$_{50}$N$_4$O$_{18}$Sm$_2$ (%): C, 45.34; H, 3.96; N, 4.41. Found: C, 45.47; H, 3.81; N, 4.54. IR (KBr, cm^{-1}): 3416(s), 1635(m), 1462(s), 1393(m), 1337(w), 1292(m), 1241(m), 1219(m), 1081(m), 962(m), 855(w), 725(m).

2.2.2. Synthesis of [Gd$_2$(MeOsaloxH)$_4$(CH$_3$COO)$_2$(H$_2$O)$_2$]·2H$_2$O (4). MeOsaloxH$_2$ (0.067 g, 0.4 mM), Gd(OAc)$_3$·4H$_2$O (0.163 g, 0.4 mM), sodium azide (0.026 g, 0.4 mM), and triethylamine (0.04 g, 0.8 mM) were dissolved in methanol (30 mL) and stirred for 4 h. Then the solution was filtered and the filtrate was left undisturbed to give yellow crystals (yield: 0.053 g, 45%, based on MeOsaloxH$_2$) of **4** [scheme 1(b)]. Anal. Calcd for C$_{36}$H$_{46}$Gd$_2$N$_4$O$_{20}$ (%): C, 36.98; H, 3.97; N, 4.79. Found: C, 37.03; H, 3.88; N, 4.67. IR (KBr, cm^{-1}): 3457(s), 1638(m), 1591(m), 1460(s), 1385(w), 1340(m), 1294(m), 1239(m), 1219(m), 1096(w), 1076(m), 960(m), 851(w), 730(m).

2.3. *Crystal structure determination*

The crystallographic parameters and the refinement statistics are listed in table 1 and the related bond lengths and angles are listed in tables 2 and 3. Diffraction measurements for **1**–**4** were carried out using a Bruker SMART-1000 CCD diffractometer with

Table 1. Crystallographic data and structure refinement parameters for **1**–**4**.

Complex/parameter	1	2	3	4
Empirical formula	C$_{48}$H$_{50}$N$_4$O$_{18}$Pr$_2$	C$_{48}$H$_{50}$N$_4$O$_{18}$Nd$_2$	C$_{48}$H$_{50}$N$_4$O$_{18}$Sm$_2$	C$_{36}$H$_{46}$N$_4$O$_{20}$Gd$_2$
Formula weight	1252.74	1259.40	1271.62	1169.27
T(K)	293(2)	298(2)	293(2)	293(2)
Crystal system	Triclinic	Triclinic	Triclinic	Triclinic
Space group	*P*-1	*P*-1	*P*-1	*P*-1
a (Å)	10.3476(11)	10.3420(9)	10.3535(14)	8.6518(5)
b (Å)	10.4125(7)	10.3570(11)	10.404(2)	10.5813(9)
c (Å)	12.6208(14)	12.5590(13)	12.530(2)	12.0475(11)
α (°)	79.062(8)	79.2470(10)	71.079(18)	103.992(8)
β (°)	71.031(10)	71.0510(10)	79.748(14)	100.461(6)
γ (°)	88.301(7)	88.384(2)	88.830(14)	90.788(6)
V (Å^3)	1261.8(2)	1249.2(2)	1255.4(4)	1050.47(15)
Z	1	1	1	1
D_c (Mg m^{-3})	1.649	1.674	1.682	1.848
μ (mm^{-1})	1.985	2.133	2.393	3.215
Data/parameters	4444/330	4332/325	4425/331	3702/285
R_{int}	0.0497	0.0806	0.0573	0.0498
GOOF (F^2)	1.066	0.981	1.043	1.046
R_1 [$I > 2\sigma(I)$]	0.0487	0.0771	0.0516	0.0456
wR_2 (all data)	0.0957	0.2074	0.0954	0.1046

Table 2. Selected bond lengths (Å) for **1**–**4**.

1		2		3		4	
Pr(1)–O(2)	2.360(4)	Nd(1)–O(2)	2.340(7)	Sm(1)–O(2)	2.330(5)	Gd(1)–O(5)	2.309(4)
Pr(1)–O(5)	2.373(4)	Nd(1)–O(5)	2.372(7)	Sm(1)–O(5)#1	2.359(5)	Gd(1)–O(2)#1	2.355(5)
Pr(1)–O(7)	2.474(4)	Nd(1)–O(9)#1	2.464(7)	Sm(1)–O(8)#1	2.426(5)	Gd(1)–O(8)#1	2.408(5)
Pr(1)–O(8)#1	2.523(4)	Nd(1)–O(5)#1	2.488(6)	Sm(1)–O(7)	2.481(5)	Gd(1)–O(7)	2.447(4)
Pr(1)–O(5)#1	2.527(3)	Nd(1)–O(8)	2.497(7)	Sm(1)–O(5)	2.488(4)	Gd(1)–O(9)	2.457(5)
Pr(1)–O(9)	2.570(4)	Nd(1)–O(7)	2.549(7)	Sm(1)–O(9)	2.522(4)	Gd(1)–O(2)	2.491(4)
Pr(1)–O(6)#1	2.629(4)	Nd(1)–O(6)	2.610(8)	Sm(1)–O(6)	2.612(5)	Gd(1)–N(1)#1	2.616(6)
Pr(1)–N(2)	2.660(5)	Nd(1)–N(2)	2.628(8)	Sm(1)–N(2)#1	2.628(6)	Gd(1)–O(3)	2.642(5)
Pr(1)–N(1)	2.675(6)	Nd(1)–N(1)	2.663(8)	Sm(1)–N(1)	2.650(6)	Gd(1)–N(2)	2.659(6)

Symmetry transformations used to generate equivalent atoms: #1 of **1**: $1 - x$, $-y$, $1 - z$; #1 of **2**: $-x$, $1 - y$, $2 - z$; #1 of **3**: $-x$, $-y$, $-z$; #1 of **4**: $1 - x$, $1 - y$, $1 - z$.

Table 3. Bond lengths (Å) and angles (°) of noncovalent interactions for **1**–**4**.

D–H···A	D–H (Å)	H···A (Å)	D···A (Å)	D–H···A (°)	Symmetry
Complex 1					
O9–H9A···O4#2	0.82	1.96	2.726(5)	154.0	$1 - x$, $1 - y$, $1 - z$
C7–H7···O1#3	0.93	2.71	3.532(9)	148.6	$1 - x$, $-y$, $2 - z$
C22–H22···O1#4	0.93	2.67	3.527(10)	154.1	$1 + x$, y, $-1 + z$
Complex 2					
O9–H9A···O4#2	0.82	1.95	2.712(10)	153.4	$-x$, $-y$, $2 - z$
C7–H7···O1#3	0.93	2.67	3.527(15)	154.2	$-x$, $1 - y$, $1 - z$
C22–H22···1#4	0.93	2.64	3.508(18)	155.1	$1 - x$, $1 - y$, $1 - z$
Complex 3					
O9–H9A···O4#2	0.82	1.99	2.748(6)	153.1	$1 + x$, y, z
C7–H7···O1#3	0.93	2.70	3.541(10)	151.5	$-x$, $-y$, $1 - z$
C22–H22···O1#4	0.93	2.67	3.533(12)	154.0	$-x$, $-1 - y$, $1 - z$
Complex 4					
O10–H10B···O6	0.85	2.03	2.876(10)	177.8	–
O10–H10A···O8#1	0.85	2.00	2.850(9)	177.5	$1 - x$, $1 - y$, $1 - z$
O9–H9B···O10#2	0.85	1.90	2.668(9)	149.7	$-1 + x$, y, z
O9–H9A···O1#3	0.85	2.08	2.856(7)	150.9	x, $-1 + y$, z
C15–H15···O4#4	0.93	2.68	3.338(11)	128.6	$1 - x$, $1 - y$, $2 - z$

graphite-monochromated Mo Kα radiation ($\lambda = 0.71073$ Å). The structures were solved by direct methods and all nonhydrogen atoms were refined anisotropically by least-squares on F^2 using the SHELXTL program [31]. Hydrogens were positioned geometrically and refined using the riding model. CCDC 966255 (**1**), 966256 (**2**), 966257 (**3**), and 966254 (**4**) contain the supplementary crystallographic data.

3. Results and discussion

3.1. *Description of structures*

3.1.1. Synthesis and crystal structures of 1–4. Four new homobinuclear lanthanide(III) complexes, [Ln$_2$(MeOsaloxH)$_4$(PhCOO)$_2$(CH$_3$OH)$_2$] (Ln = Pr, **1**; Nd, **2**; Sm, **3**) and

[Gd$_2$(MeOsaloxH)$_4$(CH$_3$COO)$_2$(H$_2$O)$_2$]·2H$_2$O (**4**), were prepared by reaction of MeOsaloxH$_2$, Ln(OAc)$_3$·nH$_2$O and PhCOONa (or NaN$_3$) in the presence of triethylamine in methanol. In **1–3**, PhCOO$^-$ coordinates to Ln^{3+} ions, while in **4**, N$_3^-$ did not bond with Gd^{3+}. We used the synthetic method of **4** to obtain a Dy$_3$ complex (Supplementary material), which was very similar to the reported Dy$_3$ complexes [26]. In this synthesis system, N$_3^-$ also did not participate in coordination to Dy^{3+}. We also tried the reactions without NaN$_3$, and the result proved that the absence of NaN$_3$ led to complexes in low yields (21%). The same experimental result has been reported [32].

X-ray crystallography indicates that **1–3** are isomorphous (figure 1) and **1** is described. Complex **1** crystallizes in the triclinic space group *P-1*. The molecule is centrosymmetric and consists of two Pr ions (Pr1 and Pr#1, #1: 1 − *x*, −*y*, 1 − *z*), four [MeOsaloxH]$^-$ ligands, two benzoate ligands, and two coordinated methanol molecules. Pr1 is nine-coordinate and exhibits a distorted tricapped trigonal prismatic coordination configuration with [N$_2$O$_7$] donor sets (figure 2). Six coordination atoms of the prism positions are provided by two [MeOsaloxH]$^-$ ligands phenolate O2 and O5, one [MeOsaloxH]$^-$ ligand methoxy O6#1, one coordinated methanol, and two benzoates (O7, O8#1). The three capping positions are occupied by a phenolate O5#1 and oxime N1 and N2 from three [MeOsaloxH]$^-$ ligands. The bond distances of Pr–O/N range from 2.359(4) to 2.674(6) Å. In **1**, four [MeOsaloxH]$^-$ ligands show two coordination modes, $\eta^1:\eta^2:\eta^1:\mu_2$ and $\eta^1:\eta^1:\mu_1$, respectively [scheme 2(a) and (b)]. In the $\eta^1:\eta^2:\eta^1:\mu_2$-[MeOsaloxH]$^-$ ligand, phenolate O5 is asymmetrically bridging the two Pr centers, with Pr1–O5 = 2.373(4) Å and Pr1#1–O5 = 2.527(3) Å, while the methoxyl O6 coordinates monodentate to Pr1#1, with Pr1#1–O6 = 2.629(4) Å (longer than the bond lengths of Pr1–O5 and Pr1#1–O5). The Pr–O (O2) bond length (2.360(4) Å)
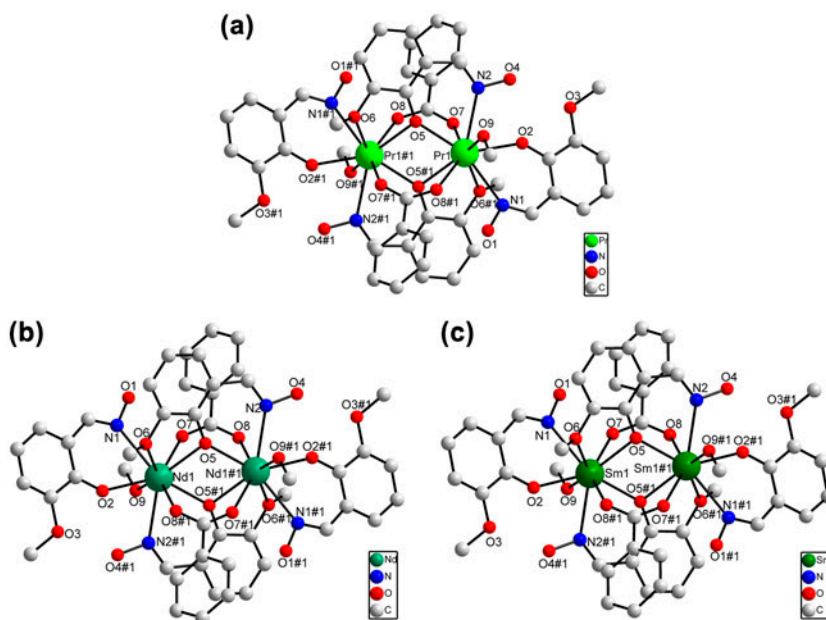

Figure 1. Molecular structures of complexes **1** (a), **2** (b) and **3** (c). All hydrogen atoms are omitted for clarity. Displacement ellipsoids are drawn at the 50% probability level (Symmetry transformations used to generate equivalent atoms: #1 of **1**: 1 − *x*, −*y*, 1 − *z*; #1 of **2**: −*x*, 1 − *y*, 2 − *z*; #1 of **3**: −*x*, −*y*, −*z*).
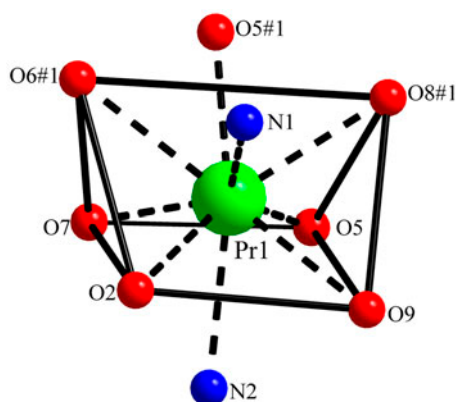
Figure 2. The distorted tricapped trigonal prismatic geometry of the Pr ion of **1**. Displacement ellipsoids are drawn at the 50% probability level.

of $\eta^1 : \eta^1 : \mu_1$-[MeOsaloxH]$^-$ is shorter than the Pr–O bond length of $\eta^1 : \eta^2 : \eta^1 : \mu_2$-[MeO-saloxH]$^-$. The benzoate adopts $\eta^1 : \eta^1 : \mu_2$ mode, bridging Pr1 and Pr1#1 [scheme 2(c)], with Pr1–O7 = 2.474(4) and Pr1#1–O8 = 2.523(4) Å. The Pr–O band distances are related with the coordination geometries of the ligands. As a result, the two Pr centers are bridged by two phenolates from two $\eta^1 : \eta^2 : \eta^1 : \mu_2$-[MeOsaloxH]$^-$ ligands and two carboxylates from a pair of $\eta^1 : \eta^1 : \mu_2$-benzoate ligands to form a [Pr$_2$O$_2$(PhCOO)$_2$] binuclear structure with two benzoate ligands on two sides of the [Pr$_2$O$_2$] plane. Within the binuclear core, the Pr$\cdots$Pr1#1 distance and Pr1–O5–Pr#1 bond angle are 3.8567(7) Å and 103.82(15)°, respectively, where the bond angle is close to previously reported bond angles, while the
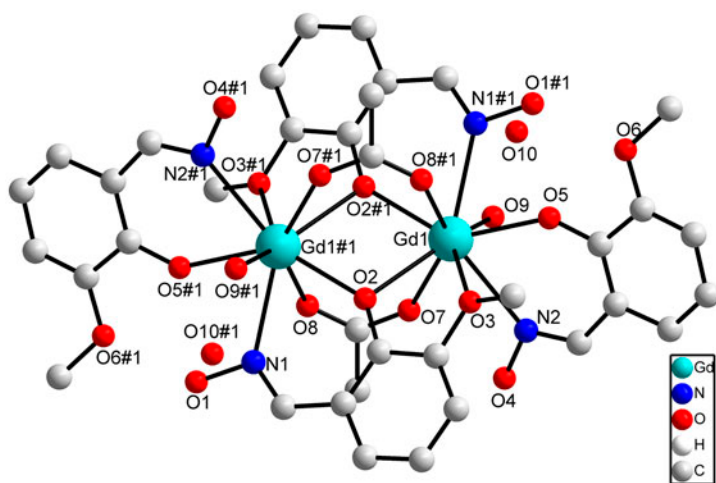

Figure 3. Molecular structure of **4**. All hydrogens are omitted for clarity. Displacement ellipsoids are drawn at the 50% probability level (Symmetry transformations used to generate equivalent atoms: #1: $1 - x$, $1 - y$, $1 - z$).

distance of Pr1⋯Pr1#1 is shorter than previously reported Pr complex $[Pr_2(C_2O_4)_2$ $(pyzc)_2(H_2O)_2]_n$ (for which Pr⋯Pr distances were 4.463(4)–6.499(1) Å, pyzcH = 2-pyrazin-ecarboxylic acid) [33].

Complex **4** exhibits similar structures to that of **1–3** (figure 3). In this case, however, acetates replace the benzoate ligands to construct the binuclear cores. Lattice water molecules were present in the structure. In the $[Gd_2O_2(CH_3COO)_2]$ binuclear structure, the bond angle of Gd1–O2–Gd#1 (#1: $1 - x$, $1 - y$, $1 - z$) is 103.66(7)° and the distance for Gd1⋯Gd1#1 is 3.811(7) Å. The Ln–O/N bond lengths (mean value 2.532 Å, **1**; 2.513 Å, **2**; 2.499 Å, **3**; 2.486 Å, **4**) and the distances for Ln⋯Ln#1 (3.8567(7) Å, **1**; 3.826 Å(10) **2**, 3.812(10) Å **3**, 3.811(7) Å, **4**) become slightly shorter with increase in atomic number, as expected due to the lanthanide contraction.

Based on MeOsaloxH$_2$, several homo-lanthanide complexes have been reported, including a Dy$_7$ cluster and a family of linear Dy$_3$ and Tb$_3$ clusters [25, 26], which were also synthesized by the solvent evaporation method. From their structure, MeOsaloxH$_2$ could easily coordinate to different rare earth metal cations to form various di- and multi-nuclear complexes with interesting structures, owing to its strong coordination ability and versatile coordination modes. In these reported complexes, there are two kinds of deprotonated MeOsaloxH$_2$ ligands: mono-deprotonated (i.e. [MeOsaloxH]$^-$) and fully deprotonated (i.e. [MeOsalox]$^{2-}$). In the Dy$_7$ cluster, [MeOsaloxH]$^-$ and [MeOsalox]$^{2-}$ show two kinds of coordination modes $\eta^1 : \eta^2 : \eta^1 : \mu_2$ for [MeOsaloxH]$^-$ and $\eta^1 : \eta^1 : \eta^2 : \mu_3$ for [MeOsalox]$^{2-}$ [scheme 2(a) and (d)]. In the family of linear Dy$_3$ and Tb$_3$ clusters, the [MeOsaloxH]$^-$ and [MeOsalox]$^{2-}$ ligands adopt three kinds of coordination modes $\eta^1 : \eta^2 : \eta^1 : \mu_2$ and $\eta^1 : \eta^1 : \mu_1$ for [MeOsaloxH]$^-$ ligands and $\eta^1 : \eta^2 : \eta^1 : \eta^1 : \mu_3$ for [MeOsalox]$^{2-}$ ligands [scheme 2(a), (b) and (e)].

Among previously reported lanthanide complexes, most Ln$_2$ clusters are based on carboxylate ligands [34–37], which were generally hydrothermally synthesized. In these complexes, carboxylate ligands mainly adopt three coordination modes $\eta^2 : \eta^1 : \mu_2$, $\eta^1 : \eta^1 : \mu_2$ and $\eta^1 : \eta^1 : \mu_1$, and the two Ln centers were bridged by $\eta^2 : \eta^1 : \mu_2$-carboxylate ligands and/ or $\eta^1 : \eta^1 : \mu_2$-carboxylate ligands to form $[Ln_2(RCOO)_n]$ ($n = 2$ or 4) binuclear structures. In our work, the two Ln centers were bridged by two phenolate oxygens from two $\eta^1 : \eta^2 : \eta^1 : \mu_2$-[MeOsaloxH]$^-$ ligands and two $\eta^1 : \eta^1 : \mu_2$-carboxylate ligands to form a $[Ln_2O_2(PhCOO)_2]$ binuclear structure. Therefore, this work expands the field of known lanthanide coordination polymers. In addition, we provide a facile synthetic route for synthesis of homobinuclear lanthanide complexes, which could be used to prepare other lanthanide(III) coordination polymers.

3.1.2. Supramolecular architectures of 1–4. Complexes **1–4** form two different types of 3-D supramolecular architectures. Complex **1** also was selected for the detailed description in **1–3**. Complex **1** shows a 3-D supramolecular architecture formed by hydrogen bonds and weak C–H⋯O interactions, with O–H⋯O hydrogen-bonding interactions linking adjacent molecules to form supramolecular chains along the *b* axis. As shown in figure 4(a), adjacent molecules are connected by O–H⋯O hydrogen-bonding interactions, which occur between the methanol hydrogen (H9A) and the oxime oxygen (O4#2, #2: $1 - x$, $1 - y$, $1 - z$) of the adjacent molecule, and extend along the *b* axis to give a supramolecular chain. These 1-D supramolecular chains are further interconnected through weak C–H⋯O interactions along two different directions to afford a 3-D supramolecular architecture. In the *ac*
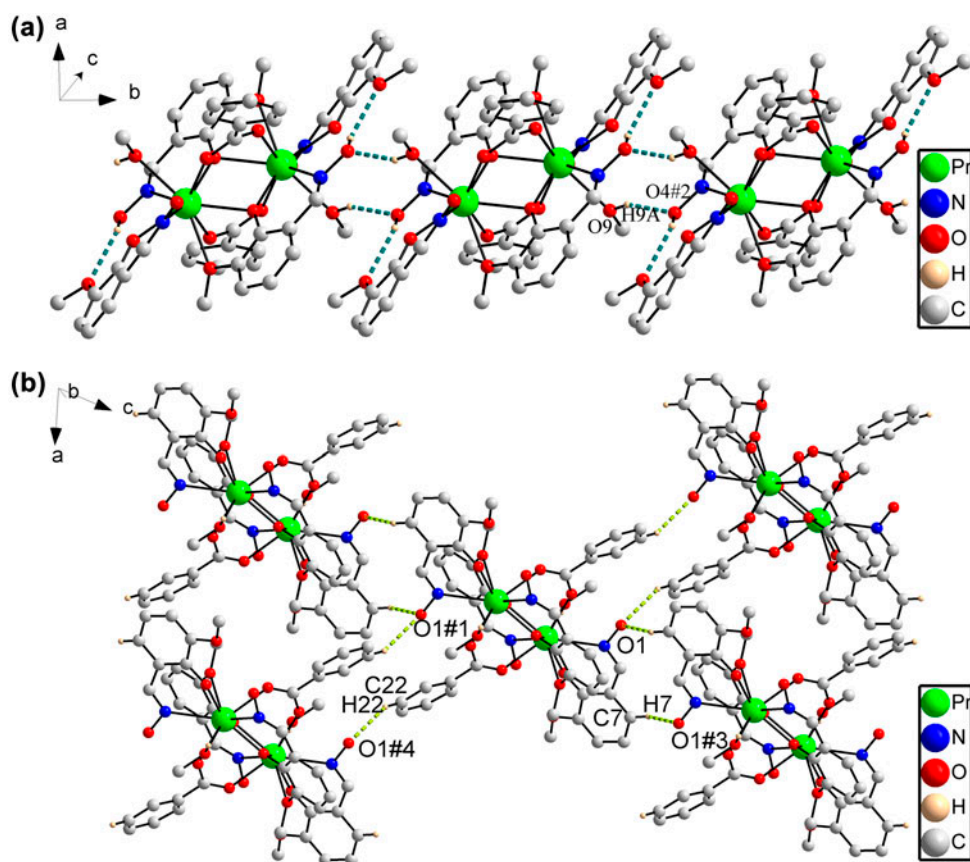
Figure 4. Hydrogen bonds of **1** along the *b* axis (a) and weak C–H···O interactions of **1** in the *ac* plane (b). Color code: hydrogen bonds, teal; weak C–H···O interactions, lime (see http://dx.doi.org/10.1080/00958972.2015.1009451 for color version).

plane, as shown in figure 4(b), each molecule links four adjacent molecules through weak C–H···O interactions; the oxygens (O1 and O1#1) involved in these interactions belong to oxime of the central molecule, while the hydrogens are derived from phenyl moiety of four adjacent molecules.

Complex **4** shows a 3-D supramolecular architecture formed by hydrogen bonds and weak C–H···O interactions, with O–H···O hydrogen-bonding interactions linking adjacent molecules to form 2-D supramolecular networks parallel to the *ab* plane. As shown in figure 5(a), there are hydrogen bonds (O10–H10A···O8#1 and O10–H10B···O6) between the Gd$_2$ cluster and free water. Among these hydrogen bonds, O10, H10A, and H10B are derived from the free water molecule, O8#1 belongs to coordinated water, and O6 belongs to methoxy of one [MeOsaloxH]$^-$. The structure is further connected by O–H···O hydrogen bond (O9–H9B···O10#2, #2: −1 + *x*, *y*, *z*) between the coordinated water and the uncoordinated H$_2$O of adjacent structure and extend along the *a* axis to give a supramolecular chain. Furthermore, adjacent supramolecular chains are further linked by hydrogen-bonding interactions which occur between the uncoordinated water (O9–H9A) and the oxime oxygen (O1#3, #3: *x*, −1 + *y*, *z*) of one [MeOsaloxH]$^-$ ligand from an adjacent molecule, and
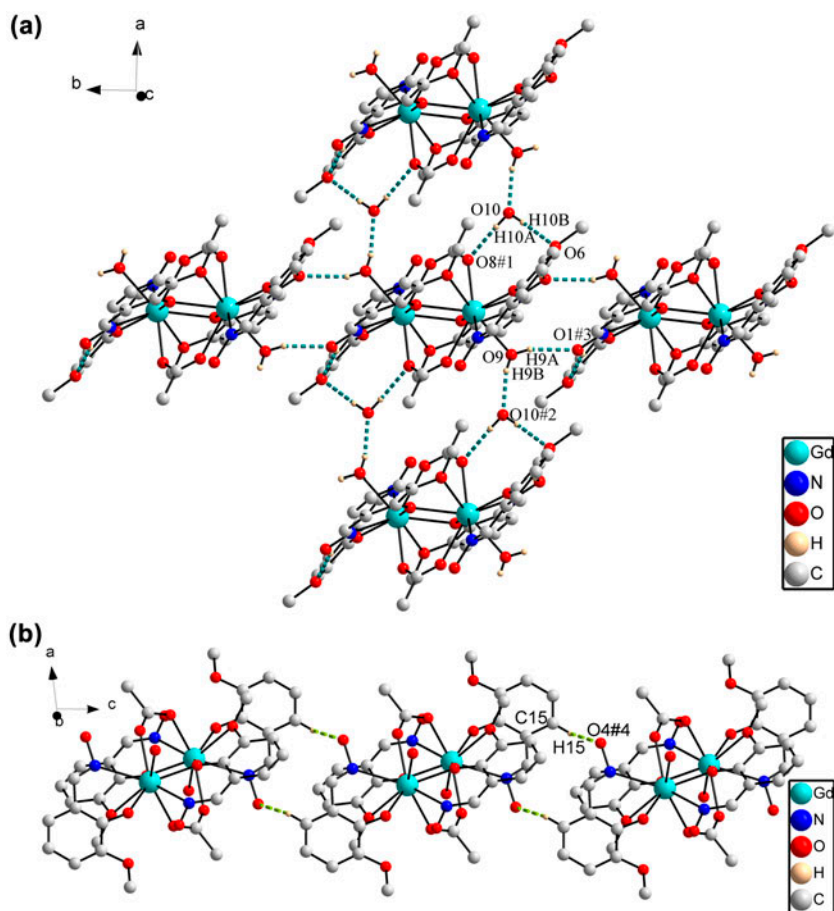
Figure 5. Hydrogen bonds of **4** along the *ab* plane (a) and weak C–H···O interactions of **4** along the *c* axis (b). Color code: hydrogen bonds, teal; weak C–H···O interactions, lime (see http://dx.doi.org/10.1080/00958972.2015.1009451 for color version).

expand along the *b* axis to yield a 2-D supramolecular network. The 2-D supramolecular networks are further interconnected through weak C–H···O interactions to afford a 3-D supramolecular architecture along the *c* axis. H15 involved in weak C–H···O interaction belongs to the phenyl moiety and O4#4 (#4: $1 - x$, $1 - y$, $2 - z$) is derived from the adjacent oxime group [figure 5(b)].

3.2. *Magnetic properties*

3.2.1. Magnetic property of 1. The effects of magnetic exchange coupling for systems containing Ln ions are much weaker than those of transition metal ions [38, 39]. For Pr^{III}, the magnetic properties of Pr^{III} ions are strongly influenced by it possessing rather large unquenched orbital angular momentum associated with the internal nature of the valence of orbitals and simultaneously have orbitally degenerate ground states, which are facile to be split by spin–orbit coupling and crystal field effects [40].

The magnetic susceptibilities of **1** and **2** were measured from 2 to 300 K as shown in figure 6. The values of $\chi_M T$ at 300 K are 3.74 and 3.63 cm^3 K M^{-1}, respectively, slightly higher than those expected (3.20(**1**) and 3.28(**2**) cm^3 K M^{-1}) for two insulated Pr^{III} ions and Nd^{III} ions. As the temperature lowers, $\chi_M T$ gradually decreases to 0.24 and 1.47 cm^3 K M^{-1} at 2 K, respectively. An analogous situation was observed for the recently reported complexes, $\{[Pr_2(PDA)_2(H_2O)_5SO_4]\cdot 2H_2O\}_n$ (PDA = pyridine-2,6-dicarboxylic anion) [40], $[Nd_2(\mu_2\text{-OOCFc})_2(OOCFc)_4(H_2O)_4]\cdot 2MeOH\cdot H_2O$ (Fc = $(\eta^5\text{-}C_5H_5)Fe(\eta^5\text{-}C_5H_4)$) [41] and $[Nd_2(\mu_2\text{-OOCCym})_4(OOCCym)_2(THF)_4]$ (Cym = $(\eta^5\text{-}C_5H_4)Mn(CO)_3$) [42]. Due to the existence of strong spin–orbit coupling for lanthanide ions, the nature of the interactions between the two Pr/Nd ions could not be unambiguously deduced from the shape of the $\chi_M T$ *versus* T curve. The decrease in $\chi_M T$ originates in the thermal depopulation of the
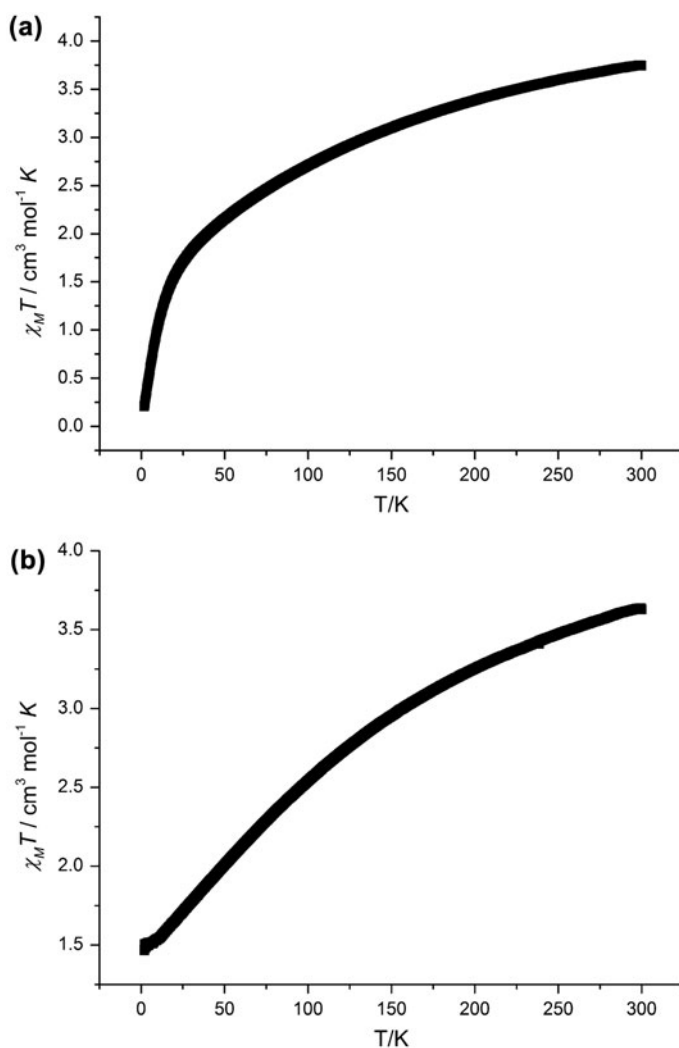

Figure 6.   Temperature dependence of $\chi_M T$ for **1** (a) and **2** (b).

highest Stark components derived from splitting of the free-ion ground state $^3H_4/^4I_{9/2}$ by the crystal field [43]. Accordingly, weak exchange interactions within the structures are masked by crystal field effects, and no conclusions could be drawn about their values and sign for these products.

3.2.2. Magnetic property of 4. Because Gd^{III} ion has the greatest possible number of unpaired electrons ($S = 7/2$) among the 4f-elements, and this is an isotropic ion for which there is no spin-orbit coupling and this eases the mathematical description of magnetic properties for its complexes. Complexes containing Gd^{III} take a special place among the complexes of 4f elements [44]. For **4**, as shown in figure 7, the value of $\chi_M T$ is 15.99 cm^3 K M^{-1} at 300 K, which is close to the theoretical value (15.86 cm^3 K M^{-1}) for two isolated Gd^{III} ions ($^8S_{7/2}$) [45]. With decreasing temperature, the value of $\chi_M T$ remains almost invariable over a broad temperature range, then decreases to 7.90 cm^3 K M^{-1} at 2 K. From 50 to 300 K, the dependence of $1/\chi$ on T is almost linear and was well described by the Curie–Weiss law [$\chi = C/(T - \theta)$] where the constants were $C = 16.181$ cm^3 K M^{-1} and $\theta = -0.189$ K.

The magnetic behavior is interpreted with an isotropic spin Hamiltonian $H = -2JS_{Gd}S_{Gd'}$ with the quantum number $S_{Gd} = S_{Gd'} = 7/2$ [46], where J represents the exchange coupling constant. Antiferromagnetic interaction between Gd^{III} ions in the dimer with the constant $J = -0.0821$ cm^{-1} (calculated for $g = 2$) was shown. The antiferromagnetic interaction is close to that of the earlier reported gadolinium complex [Gd$_2$(μ-O,η^2-OOCCym)$_4$(η^2-OOC-Cym)$_2$(py)$_4$]·2py (for which $J = -0.0649$ cm^{-1}) [44] and stronger than that of [Gd$_2$(μ_2-OOCCym)$_4$(η^2-OOCCym)$_2$(THF)$_4$]·THF (for which $J = -0.0282$ cm^{-1}) [43], where Cym = (η^5-C$_5$H$_4$)Mn(CO)$_3$.

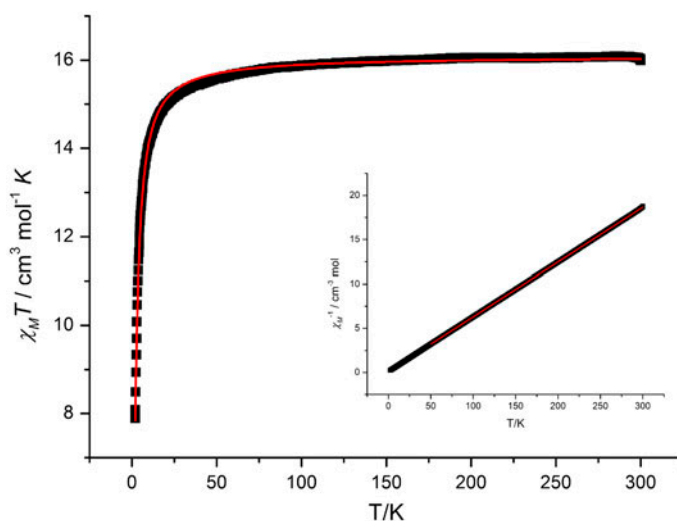

Figure 7. Temperature dependence of $\chi_M T$ and χ_M^{-1} (inset) for **4**. Color code: measured values, black; calculated curve, red (see http://dx.doi.org/10.1080/00958972.2015.1009451 for color version).

3.3. *Luminescence properties*

The solid-state photoluminescent properties of **1** and **3** have been investigated at room temperature in the visible region. Their emission spectra are shown in figure 8. The emission spectrum of **1** at excitation wavelength of 324 nm is shown in figure 8(a). There is an intense fluorescence emission at $\lambda_{max} = 617$ nm, which is associated with the $^1D_2 \rightarrow {}^3H_4$ transitions of Pr^{III}. Upon excitation at 370 nm, **3** displays three characteristic peaks of Sm^{III} in the visible region [figure 8(b)], which are attributed to $^4G_{5/2} \rightarrow {}^6H_J$ ($J = 5/2, 7/2, 9/2$), $^4G_{5/2} \rightarrow {}^6H_{5/2}$ (562 nm), $^4G_{5/2} \rightarrow {}^6H_{7/2}$ (597 nm), and $^4G_{5/2} \rightarrow {}^6H_{9/2}$ (644 nm) transitions [47].
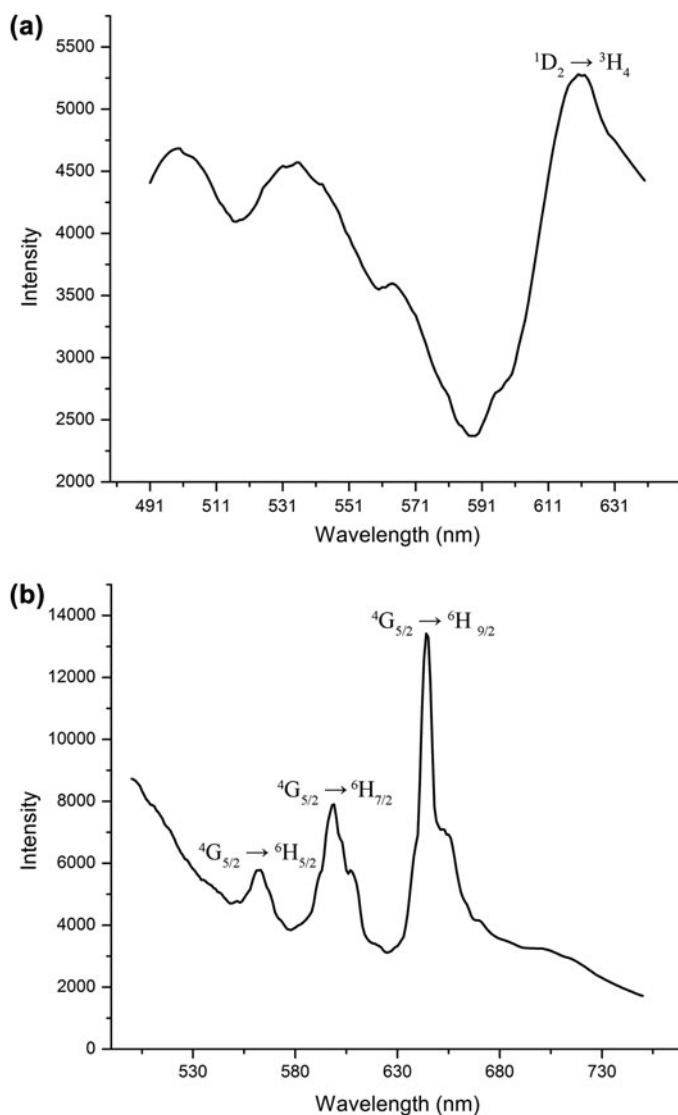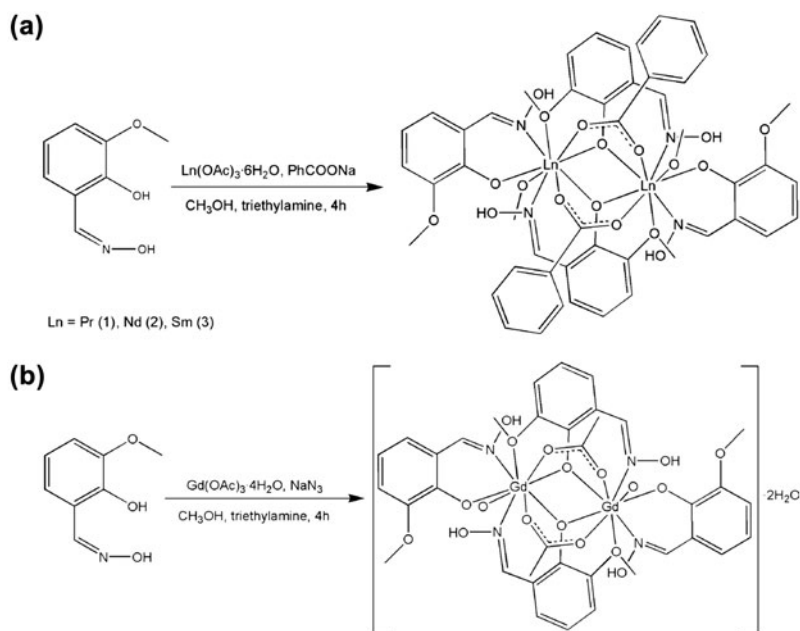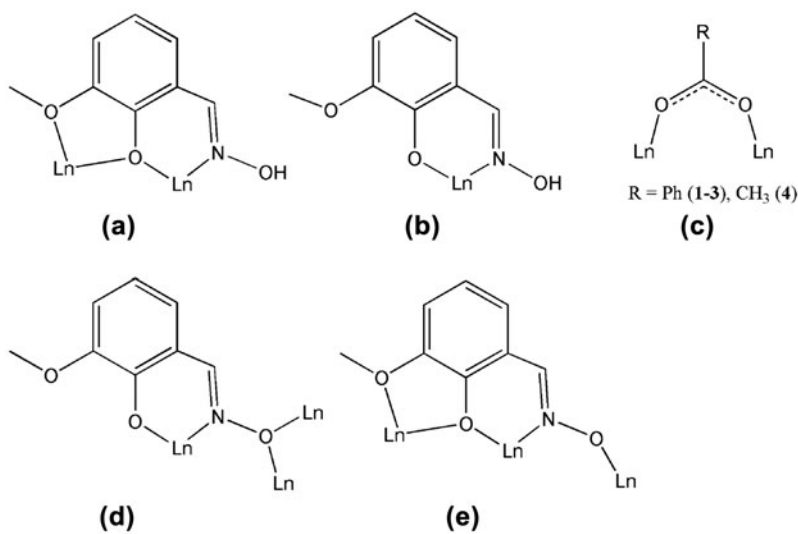

Figure 8.   Solid-state emission spectra of **1** (a) and **3** (b) at room temperature.

Scheme 1.　Synthesis of **1–3** (a) and **4** (b).

Scheme 2.　Coordination modes of the [MeOsaloxH]⁻ (a and b), auxiliary ligands (c) and [MeOsalox]²⁻ (d and e).

4. Conclusion

We have prepared four homobinuclear lanthanide(III) complexes based on 3-meth-yloxysalicylaldoxime, $[Ln_2(MeOsaloxH)_4(PhCOO)_2(CH_3OH)_2]$, where Ln = Pr (**1**), Nd (**2**), Sm (**3**) and $[Gd_2(MeOsaloxH)_4(CH_3COO)_2(H_2O)_2]\cdot2H_2O$ (**4**). In these complexes, the two Ln^{III} ions are bridged by two $O_{phenolate}$ from two $\eta^1:\eta^2:\eta^1:\mu_2$-$[MeOsaloxH]^-$ ligands and by two carboxylates to form a $[Ln_2O_2(RCOO)_2]$ binuclear structure (R = Ph, **1–3**; CH_3, **4**). Noncovalent interactions such as hydrogen bonds and weak C–H⋯O interactions in the crystal structures led to two types of 3-D supramolecular architectures. The magnetic behaviors of **1**, **2** and **4** have been studied with **4** indicative of antiferromagnetic interactions between Gd^{III} ions in the binuclear structure. Complexes **1** and **3** exhibited luminescence in the visible region. This work expands the field of homo-lanthanide coordination polymers and the self-assembly networks of lanthanide complexes.

Funding

Supplemental data

Supplemental data for this article can be accessed here [http://dx.doi.org/10.1080/00958972.2015.1009451].

References

[1] L.L. Liang, X.L. Ni, Y. Zhao, K. Chen, X. Xiao, Y.Q. Zhang, C. Redshaw, Q.J. Zhu, S.F. Xue, Z. Tao. *Inorg. Chem.*, **52**, 1909 (2013).
[2] K. Harris, Q.F. Sun, S. Sato, M. Fujita. *J. Am. Chem. Soc.*, **135**, 12497 (2013).
[3] H. Kuang, W. Ma, L. Xu, L.B. Wang, C.L. Xu. *Acc. Chem. Res.*, **46**, 2341 (2013).
[4] J.H. Deng, D.C. Zhong, X.Z. Luo, H.J. Liu, T.B. Lu. *Cryst. Growth Des.*, **12**, 4861 (2012).
[5] S.R. Batten, S.M. Neville, D.R. Turner. *Coordination Polymers: Design, Analysis and Application*, Royal Society of Chemistry, Cambridge (2009).
[6] J.W. Steed, J.L. Atwood. *Supramolecular Chemistry*, 2nd Edn, Wiley, Chichester (2009).
[7] F. Jin, Y. Zhang, H.Z. Wang, H.Z. Zhu, Y. Yan, J. Zhang, J.Y. Wu, Y.P. Tian, H.P. Zhou. *Cryst. Growth Des.*, **13**, 1978 (2013).
[8] Y.P. Xie, J. Yang, J.F. Ma, J.C. Ma, L.P. Zhang, Z.F. Jia, Z.M. Su. *Cryst. Growth Des.*, **9**, 3881 (2009).
[9] A. Gogoi, G. Das. *Cryst. Growth Des.*, **12**, 4012 (2012).
[10] T.M. Simeon, M.A. Ratner, G.C. Schatz. *J. Phys. Chem. A*, **117**, 7918 (2013).
[11] Z.Y. Zhang, Z.P. Deng, L.H. Huo, H. Zhao, S. Gao. *Inorg. Chem.*, **52**, 5914 (2013).
[12] V. Chandrasekhar, S. Kundu, J. Kumar, S. Verma, K. Gopal, A. Chaturbedi, K. Subramaniam. *Cryst. Growth Des.*, **13**, 1665 (2013).
[13] K.A. Stevenson, C.F.C. Melan, O. Fleischel, R. Wang, A. Petitjean. *Cryst. Growth Des.*, **12**, 5169 (2012).
[14] B. Notash, N. Safari, H.R. Khavasi. *Inorg. Chem.*, **49**, 11415 (2010).
[15] L. Ni, F. Hussain, B. Spingler, S. Weyeneth, G.R. Patzke. *Inorg. Chem.*, **50**, 4944 (2011).
[16] S.Y. Lin, W. Wernsdorfer, L. Ungur, A.K. Powell, Y.N. Guo, J. Tang, L. Zhao, L.F. Chibotaru, H.J. Zhang. *Angew. Chem. Int. Ed.*, **51**, 12767 (2012).
[17] P. Zhang, Y.N. Guo, J. Tang. *Coord. Chem. Rev.*, **257**, 1728 (2013).
[18] Y.N. Guo, G.F. Xu, P. Gamez, L. Zhao, S.Y. Lin, R. Deng, J. Tang, H.J. Zhang. *J. Am. Chem. Soc.*, **132**, 8538 (2010).
[19] Y.N. Guo, G.F. Xu, W. Wernsdorfer, L. Ungur, Y. Guo, J. Tang, H.J. Zhang, L.F. Chibotaru, A.K. Powell. *J. Am. Chem. Soc.*, **133**, 11948 (2011).
[20] C.H. Zhan, F. Wang, Y. Kang, J. Zhang. *Inorg. Chem.*, **51**, 523 (2012).
[21] Z. Xia, X.M. Wang, Y.X. Wang, L.B. Liao, X.P. Jing. *Inorg. Chem.*, **50**, 10134 (2011).

[22] H. Tsukube, S. Shinoda. *Chem. Rev.*, **102**, 2389 (2002).
[23] A.K. Cheetham, G. Férey, T. Loiseau. *Angew. Chem. Int. Ed.*, **38**, 3268 (1999).
[24] S. Muniappan, S. Lipstman, S. George, I. Goldberg. *Inorg. Chem.*, **46**, 5544 (2007).
[25] F.S. Guo, P.H. Guo, Z.S. Meng, M.L. Tong. *Polyhedron*, **30**, 3079 (2011).
[26] F.S. Guo, J.L. Liu, J.D. Leng, Z.S. Meng, Z.J. Lin, M.L. Tong, S. Gao, L. Ungur, L.F. Chibotaru. *Chem. Eur. J.*, **17**, 2458 (2011).
[27] R. Sekiya, S.I. Nishikiori. *Cryst. Growth Des.*, **11**, 5574 (2011).
[28] Z. Chen, M. Jia, Z. Zhang, F. Liang. *Cryst. Growth Des.*, **10**, 4806 (2010).
[29] T. Xu, L.Z. Li, H.W. Ji. *Chin. J. Synth. Chem.*, **1**, 22 (2004).
[30] P.P. Yang, X.F. Gao, H.B. Song, S. Zhang, X.L. Mei, L.C. Li, D.Z. Liao. *Inorg. Chem.*, **50**, 720 (2011).
[31] *SHELXTL 6.10*, Bruker Analytical Instrumentation, Madison, WI (2000).
[32] J.P. Tong, F. Shao, J. Tao, R.B. Huang, L.S. Zheng. *Inorg. Chem.*, **50**, 2067 (2011).
[33] B. Li, W. Gu, L.Z. Zhang, J. Qu, Z.P. Ma, X. Liu, D.Z. Liao. *Inorg. Chem.*, **45**, 10425 (2006).
[34] Z.J. Xiahou, Y.L. Wang, Q.Y. Liu, L.Q. Li, L.J. Zhou. *J. Coord. Chem.*, **66**, 2910 (2013).
[35] R. Shyni, S. Biju, M.L.P. Reddy, A.H. Cowley, M. Findlater. *Inorg. Chem.*, **46**, 11025 (2007).
[36] G.B. Che, X.C. Wang, C.B. Liu, J. Chen, S.S. Wang, X.Y. Li. *J. Coord. Chem.*, **65**, 4185 (2012).
[37] Z.V. Dobrokhotova, I.G. Fomina, G.G. Aleksandrov, Y.A. Velikodnyi, V.N. Ikorskii, A.S. Bogomyakov, L.N. Puntus, V.M. Novotortsev, I.L. Eremenko. *Russ. J. Inorg. Chem.*, **54**, 668 (2009).
[38] C. Lescop, D. Luneau, P. Rey, G. Bussière, C. Reber. *Inorg. Chem.*, **41**, 5566 (2002).
[39] W. Huang, D.Y. Wu, P. Zhou, W. Yan, D. Guo, C.Y. Duan, Q.J. Meng. *Cryst. Growth Des.*, **9**, 1361 (2009).
[40] B. Zhao, L. Yi, Y. Dai, X.Y. Chen, P. Cheng, D.Z. Liao, S.P. Yan, Z.H. Jiang. *Inorg. Chem.*, **44**, 911 (2005).
[41] H. Hou, G. Li, L. Li, Y. Zhu, X. Meng, Y. Fan. *Inorg. Chem.*, **42**, 428 (2003).
[42] P.S. Koroteev, M.A. Kiskin, Z.V. Dobrokhotova, A.S. Bogomyakov, N.N. Efimov, V.M. Novotortsev. *Polyhedron*, **30**, 2523 (2011).
[43] J.-P. Costes, J.M. Clemente-Juan, F. Dahan, F. Nicodème, M. Verelst. *Angew. Chem. Int. Ed.*, **41**, 323 (2002).
[44] P.S. Koroteev, Z.V. Dobrokhotova, M.A. Kiskin, A.S. Lermontov, N.N. Efimov, A.S. Bogomyakov, A.V. Tyurin, M.A. Bykov, L.I. Demina, YuA Velikodny, S.A. Kozyukhin, V.M. Novotortsev. *Polyhedron*, **43**, 36 (2012).
[45] C. Benelli, D. Gatteschi. *Chem. Rev.*, **102**, 2369 (2002).
[46] S.T. Hatscher, W. Urland. *Angew. Chem. Int. Ed.*, **42**, 2862 (2003).
[47] Y.Y. Zhu, Z.G. Sun, H. Chen, J. Zhang, Y. Zhao, N. Zhang, L. Liu, X. Lu, W.N. Wang, F. Tong, L.C. Zhang. *Cryst. Growth Des.*, **9**, 3228 (2009).